Energy Storage Materials 33 (2020) 108–115

Contents lists available at ScienceDirect

Energy Storage Materials

journal homepage: www.elsevier.com/locate/ensm

High performance stretchable Li-ion microbattery

Mohamed Nasreldin [a], Roger Delattre [a], Cyril Calmes [a], Marc Ramuz [a], Vinsensia Ade Sugiawati [a], Sébastien Maria [b,c], Jean-Louis de Bougrenet de la Tocnaye [d], Thierry Djenizian [a,e,*]

[a] Mines Saint-Etienne, Center of Microelectronics in Provence, Department of Flexible Electronics, F-13541, Gardanne, France
[b] Aix-Marseille Université, CNRS, UMR 7273, Inst Chim Radicalaire, F-43397, Marseille, France
[c] Réseau sur le Stockage Electrochimique de l'Energie (RS2E), FR CNRS 3459, 33 rue Saint Leu, 80039 Amiens, France
[d] IMT-Atlantique, Optics & Electronics Departments, CS 83818, F-29238, Brest, Cedex 3, France
[e] Al-Farabi Kazakh National University, Center of Physical-Chemical Methods of Research and Analysis, Tole bi str, 96A, Almaty, Kazakhstan

ARTICLE INFO

Keywords:
Stretchable microbatteries
Serpentine current collectors
Microstructured electrodes
Li-ion technology
Wearable microelectronics

ABSTRACT

The recent advances in wearable technologies had caused a surge in the demand for stretchable Li-ion microbatteries. Herein, a special design based on micropillar electrodes supported on metallic serpentines has been investigated to achieve the fabrication of a functionning device. Besides achieving high areal capacity values like 2.5 mA h cm^{-2} at C/10 (*i.e.* 0.07 mA cm^{-2}), the micropillars make the system reversibly stretchable. Electrochemical tests revealed excellent performance when the stretchable micropower source was subjected to different mechanical strains. Indeed, 73% of the capacity is retained over 100 cycles under 30% strain and all fatigue tests showed that capacity retention remain higher than 70%.

1. Introduction

Small power sources consisted of thin-films such as all-solid-state microbatteries have attracted attention to ensure autonomy of devices for wearable microelectronics and Internet of Things (IoT) [1–3]. However, the very limited mechanical deformations achieved by these rigid elements [4–8] make them unsuitable for some applications like in soft electronics, biomedical patches, The technological challenge is to design energy storage devices showing high electrochemical performance with advanced mechanical properties to prevent crack-induced deformation and subsequent loss of electrical contact. Thus, several approaches have been proposed for developing flexible microbatteries such as paper-like configuration [9–12], sponge/porous structures [13–15], and textile batteries [16–20]. As the extensible capability of these designs remains very poor, other configurations have been reported to increase the stretchability of the microbatteries including fiber shaped [21], 3D porous sponge [22,23], origami [24], wavy, [25], arched electrodes [26], honeycomb architecture [27], and serpentines formed from helical springs [28]. To prevent cracking issues under tensile strains, metallic interconnects in the form of serpentine were used to establish stretchable electrical contact between thin-film electrodes [29]. However, for such a bridge-island battery design, most of the surface is required for connections and only 28% of the substrate is occupied by the active materials. Thus, it is important to investigate and combine different strategies to achieve the fabrication of stretchable microbatteries delivering high energy and power densities. We report in the present study the conception of a new high performance stretchable Li-ion microbattery. The original aspect of the approach relies on the assembling of two stretchable substrates carrying arrays of micropillar electrodes (anode and cathode) supported on metallic serpentines that are separated by a polymer electrolyte (see the schematic representation in Fig. 1a).

The present approach reveals several advantages: i) a large covering of the stretchable substrate by the active materials, it can be over 70%. ii) Unlike compact thin-films, micropillar electrodes present empty spaces that can prevent the fracture of the materials and the formation of cracks at the electrode/current collector related to the mechanical strains and the volume variations of the electrodes during insertion/extraction of Li^+. iii) 3D microstructured electrodes also increase the energy and power densities of the microbattery owing to the larger surface area established between the electrodes and the electrolyte. This surface enhancement corresponding to the ratio between the surface of the microstructured electrode (S_{3D}) and its planar counterpart (S_{2D}) can be quantified and will be named 3D gain factor (G_{3D}). As a first approximation, the theoretical G_{3D} can be estimated according to Fig. 1b and Equation (1).

* Corresponding author. Mines Saint-Etienne, Center of Microelectronics in Provence, Department of Flexible Electronics, F-13541, Gardanne, France.
E-mail address: thierry.djenizian@emse.fr (T. Djenizian).

https://doi.org/10.1016/j.ensm.2020.07.005
Received 28 March 2020; Received in revised form 26 June 2020; Accepted 5 July 2020
Available online 7 August 2020

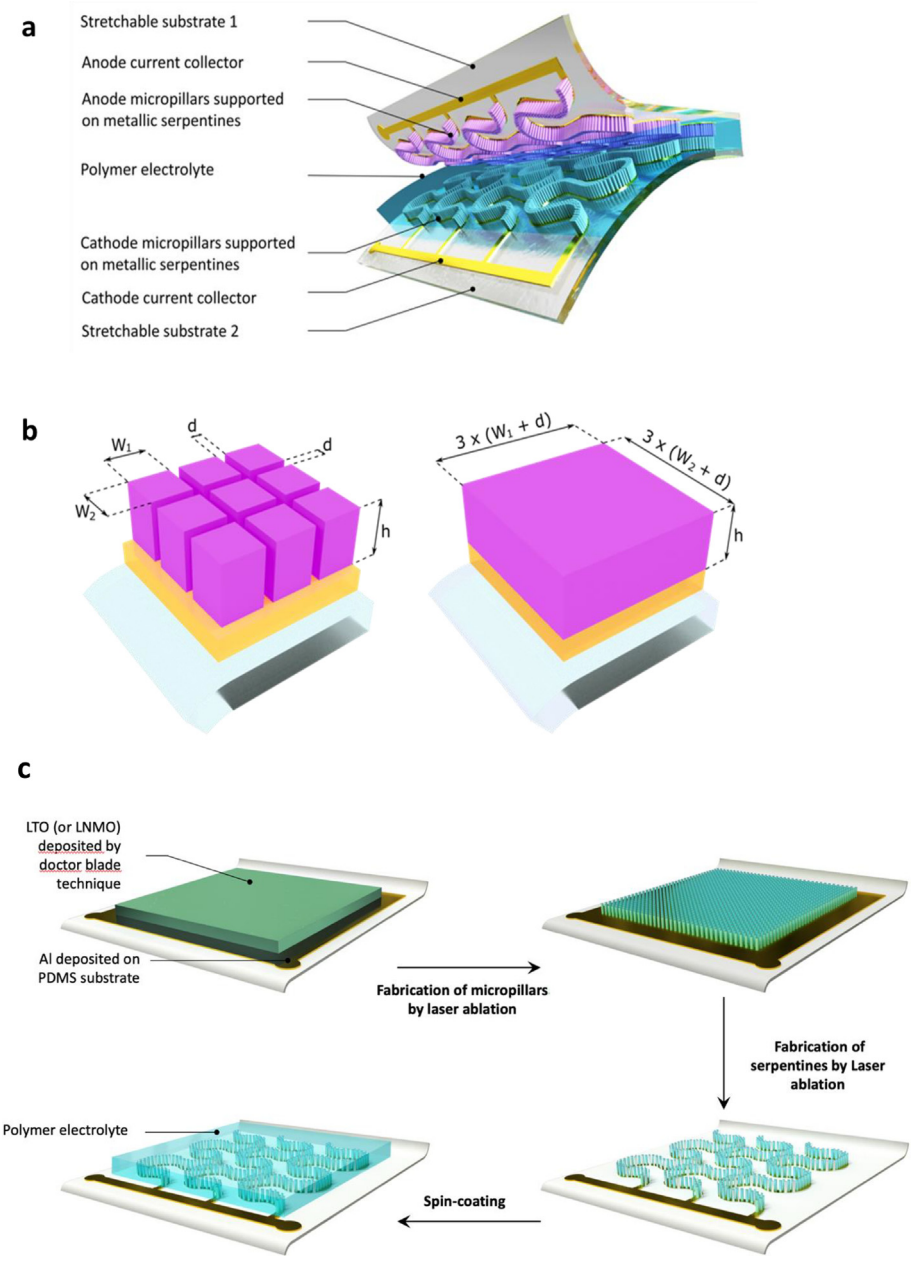

Fig. 1. a) Schematic view of the stretchable Li-ion microbattery. b) Geometrical surfaces that are considered to estimate G_{3D} by electrode microstructuring. c) Main steps proposed for the fabrication of micropillar electrodes supported on Al serpentines.

$$G_{3D} = \frac{S_{3D}}{S_{2D}} = \frac{w_1 w_2 + 2h(w_1 + w_2)}{(w_1 + d)(w_2 + d)} \quad (1)$$

Where w_1, w_2 are the sides, h the height, and d the distance spacing of the micropillars.

Due to enhanced characteristics such as high energy and power densities as well as long lifetime under multiple engineering strains, the design proposed in this work is supposed to lead to stretchable batteries able to compete with different other systems [30,31].

2. Material and methods

Thermal release double sided 90 °C Nitto RevAlpha tape, polydimethylsiloxane PDMS (Sylgard 184), Carbon black (Super P), polyvinylidene fluoride (PVDF), Lithium bis(trifluoromethanesulfonyl)imide (LiTFSI), and methyl ether methacrylate-polyethylene glycol (MA-PEG) were purchased from Sigma Aldrich, France. $LiNi_{0.5}Mn_{1.5}O_4$ (LNMO) and $Li_4Ti_5O_{12}$ (LTO) powders were purchased from MTI Corp, USA. First, PDMS thin layers were spin-coated on clean Al foils before casting the composite electrodes. For the electrode fabrication, the active powder was mixed with carbon black (Super P) and PVDF in the ratio of 90:5:5 and grounded in a mortar for 20 min. Then, the composite powder was mixed with N-methyl-2-pyrrolidone (NMP) to obtain a paste that was doctor bladed on top of the Al foil. Then, electrodes were dried under vacuum at 120 °C for 12 h to achieve a thickness of 100 μm. Micropillars and serpentines were fabricated by the laser ablation technique in a two-step procedure using the LPKF ProtoLaser S. The laser treatments were performed using a radiation of 1064 nm, a frequency of 75 kHz, and a beam diameter of 25 μm. First, a laser power of 3 W was selected to design micropillars with sides of 100 μm and a spacing of 25 μm without altering the underlying Al layer. Second, serpentine lines were patterned using a laser power of 10 W before removing the undesired regions from the PDMS. The polymer electrolyte composed of 0.5 M of LiTFSI in MA-PEG500 (with an optimized EO:Li molar ratio of 9:1) was spin-coated on

each electrode. For more clarity, a schematic representation of the fabrication process is given in Fig. 1c). It can be noted that other polymer electrolytes could be also envisioned [32–35]. The electrodes were then dried at 75 °C under vacuum for 20 h to obtain an homogeneous polymer thin-film. All microbatteries were assembled in an argon filled glove box (Jacomex) with <0.5 ppm H_2O and <0.5 ppm O_2 atmosphere. The microbatteries were then encapsulated by a PDMS layer. The galvanostatic charge/discharge measurements were carried out using a VMP3 potentiostat-galvanostat (Bio Logic). The batteries were cycled at different C-rate, where C/*n* means the battery is fully charged or discharged up to its total storage capacity in *n* hours. The stretching properties were tested using a homemade machine based on igus linear guide with reference dryline SHT. Morphological features were examined using a CARL ZEISS-S/Ultra 55 scanning electron microscope (SEM) and the chemical mapping of the surface was analyzed by Electron Dispersive X-Ray Spectrocopy (EDS). All facilities are located in a cleanroom and microbatteries were fabricated and tested at a constant temperature of 298 K.

3. Results and discussion

Fig. 2a shows the optical image of a prototype stretchable Li-ion microbattery with an entire thickness of 1.6 mm. It is composed of two distinct PDMS substrates carrying arrays of Al serpentines onto which LNMO micropillars (cathode) and LTO micropillars (anode) have been separately fabricated. For confirmation, see e.g. the SEM cross section and the EDS chemical mapping of an Al serpentine portion supporting LTO micropillars provided in Fig. S1. In addition to good electrochemical properties, these electrodes materials were chosen due to their very low volume variations during lithiation/delithiation processes, *i.e.* below 7% for LNMO and almost zero for LTO [36,37]. Thus, these materials can

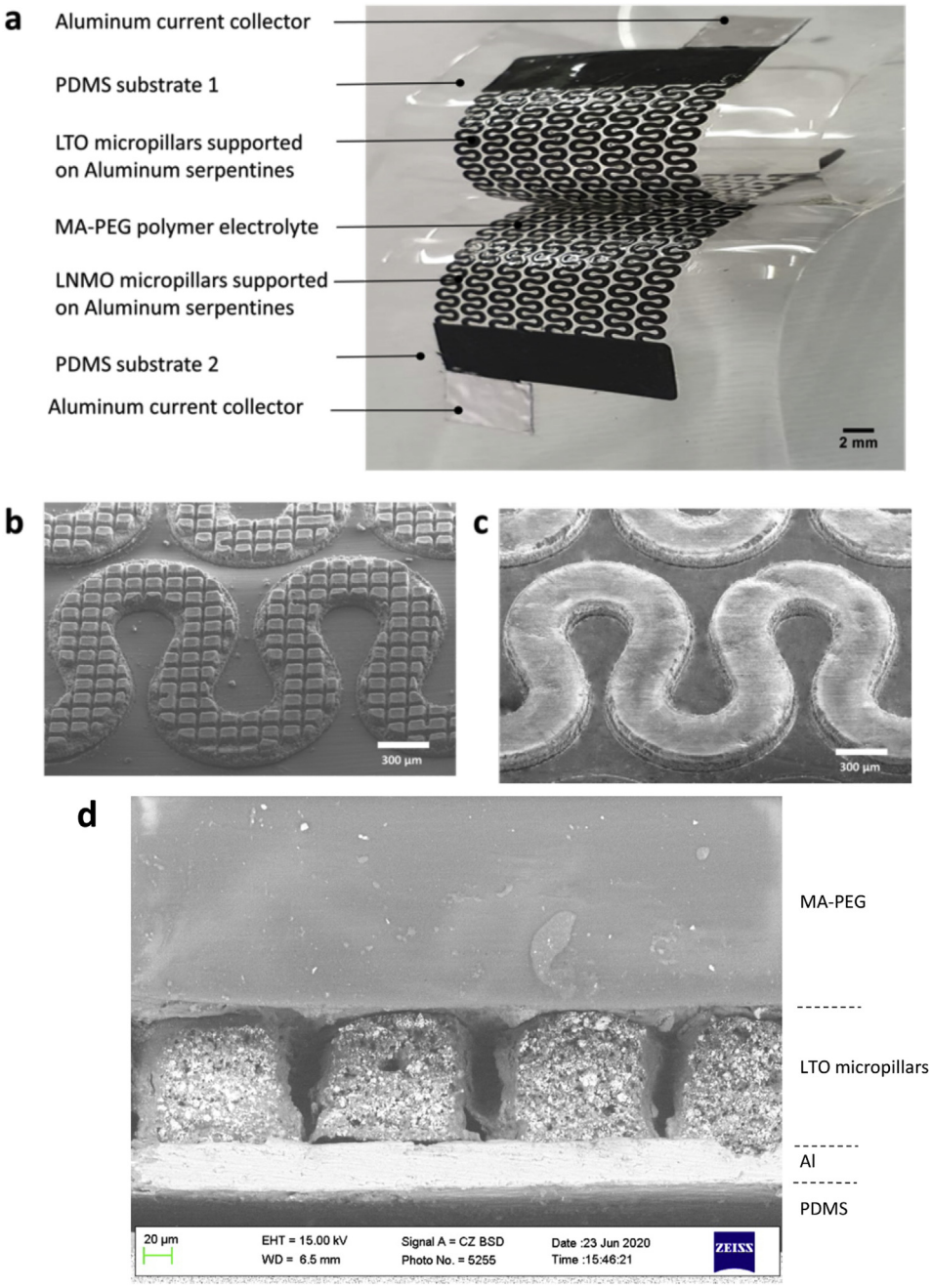

Fig. 2. a) Optical image of the prototype stretchable Li-ion microbattery. SEM images of Al serpentines supporting LNMO electrodes as b) micropillars and c) continuous film. d) Cross section view of a full battery part d).

ensure very limited structural modifications during electrochemical cycling tests. The two electrodes were separated by a spin-coated MA-PEG 500 layer that were 100 μm thick. Besides adequate mechanical properties, MA-PEG 500 carrying LiTFSI salt was selected because of several advantages: high ionic conductivity (~4×10^{-4} S cm^{-1} at room temperature, see the Arrhenius plot in Fig. S2), thermal stability up to 130 °C, low residual water content (ca. 5%) [38]. In addition, polyester based electrolytes do not suffer from decomposition as it has been highlighted for polycarbonates (depolymerization process) [39]. This microbattery will be referred to as 3D microbattery in the text. According to the experimental conditions ($w_1 = w_2 = h = 100$ μm and $d = 25$ μm), the theoretical G_{3D} value should be equal to 3.2. In order to demonstrate the benefit of the micropillars on the electrochemical and mechanical properties of the 3D microbattery, another stretchable system based on planar LTO and LNMO electrodes supported on metallic serpentines were also fabricated and will be referred to as 2D microbattery. Fig. 2b and c shows the SEM images of micropillar (3D) and planar (2D) LNMO electrodes supported on Al serpentines. The cross section view of a full battery part has been also examined by SEM (Fig. 2d). This result revealed that the two electrodes are well separated but the polymer does not completely line the micropillar walls.

Fig. 3a shows the charge/discharge profile of the 3D microbattery in a potential window of 1 V–3.5 V at C/10 (*i.e.* 0.07 mA cm^{-2}) for 10 cycles. The operating voltage is equal to 2.55 V due to the reversible intercalation of the Li^+ in LTO and LNMO at 1.55 V and 4.7 V vs. Li/Li^+, respectively. The areal discharge capacities for the 1st, 2nd, and 10th cycles are 2.51 mA h cm^{-2}, 2.30 mA h cm^{-2}, and 2.20 mA h cm^{-2}, respectively. The 1st irreversibly capacity which is only 0.21 mA h cm^{-2}, can be attributed to side reactions (e.g. Li^+ with residual water) and/or the formation of a Solid Electrolyte Interphase (SEI) layer at the surface of the anode. The capacity retention between the 2nd and 10th cycle is 96% and the coulombic efficiency (CE) varies from 97.8% to 97.6%. In order to highlight the strong advantages of using micropillars over continuous film on the electrochemical performance of the batteries, the 2D microbattery was also characterized by galvanostatic cycling tests under the same conditions (Fig. 3b). Clearly, lower areal capacities are obtained for the 2D configuration: 0.94 mA h cm^{-2} (1st cycle), 0.92 mA h cm^{-2} (2nd cycle), and 0.87 mA h cm^{-2} (10th cycle). The capacity

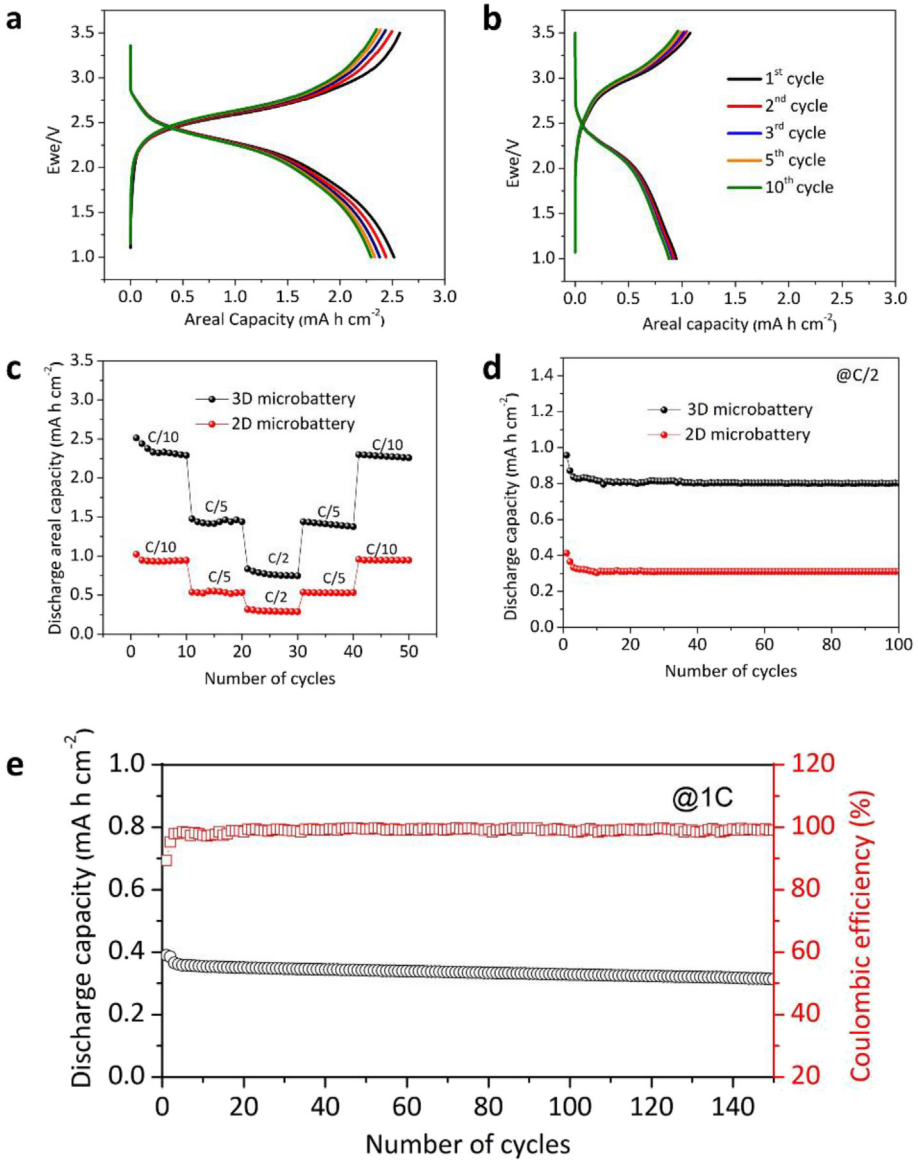

Fig. 3. Galvanostatic charge/discharge profiles of a) 3D microbattery b) 2D microbattery. c) Electrochemical performance of the two microbatteries at multi C-rates. d) Discharge capacity values of the two microbatteries for 100 cycles at C/2 rate. e) Discharge capacity values and coulombic efficiency variations of the 3D microbattery for 150 cycle at 1C.

retention achieved is also a bit weaker (94%) just like for the CE ranging from 87.8% to 93.0%. From these results, the magnitudes of areal capacities of the 3D microbattery are around 2.5 times higher than that of the 2D microbattery, which corresponds to ca. 78% of the theoretical G_{3D}. The difference between the theoretical value and the experimental result can be attributed to two effects. First, the achieved electrolyte/electrolyte interface as the micropillars are not conformally coated by the polymer electrolyte (Fig. 2d). Second, the laser ablation technique as some micropillars are missing on the edges of the serpentines (see Fig. 2b) and the upper part of the micropillars are not vertical but flared (see the SEM cross section of LTO micropillars in Fig. S2). The positive influence of the micropillar geometry on the electrochemical performance of the microbatteries is definitely associated to the 3D gain factor, which is responsible for the largest contact surface area established between the active materials and the electrolyte. Beyond the improvement of the areal capacity values, the presence of microstructures could improve the capacity retention and the CE as well. These results are in accordance with literature [40,41]. Indeed, 3D vertical microstructures ensure a dramatic improvement in surface-to-volume ratio without a subsequent increase in overall volume. They are separated by voids that are efficient to mitigate the volume variation of materials (for less mechanical strains) and provide more space and paths for the electrolyte penetration (for more exchanges of Li ions through a better electrode/electrolyte interface). It has been also reported that electric field distribution along vertical pillars (and therefore the corresponding current density) is larger at the edge of the electrodes [42]. All these effects are responsible for the enhancement of the kinetics and performance of 3D electrodes.

Fig. 3c shows the electrochemical cycling performance of the 3D and the 2D microbatteries at different kinetics for 50 cycles. First, the discharge capacities obtained at various rates reveal a good stability. Second, the areal capacities are retrieved at C/10 after tests performed at C/5 and C/2 attesting the excellent chemical properties of the battery compounds. In addition, G_{3D} remains in the same order than that obtained at C/10, ca. 2.5 confirming the advantage of using microstructured electrodes with high specific surface area.

Fig. 3d shows the long-term cycling behavior of the 3D and 2D microbatteries at C/2 for 100 cycles. Beyond the remarkably high stability of the discharge capacity values obtained from the two systems, the 3D microbattery reveals a capacity retention of 92% between the 2nd and the 100th cycle with $G_{3D} = 2.6$ for the last cycle. The excellent electrochemical performance of the 3D design is also demonstrated at 1C up to 150 cycles with a final capacity retention of 81% and CE values varying from 89.4% to 99.0% (Fig. 3e). All the above results confirm that the micropillar geometry increased the electrochemical performance by 2.5 times, which is in agreement with the estimation of G_{3D}.

The main characteristics for the planar and 3D microbatteries are summarized in Table 1.

It can be noticed that the performance of the battery could be optimized by decreasing the micropillar size. According to Equation (1), the maximal theoretical 3D gain factor equal to 4.26 can be reached for micropillars of 29 μm side (assuming a height of 100 μm and a spacing of 25 μm that corresponds to the smallest laser beam diameter).

Although serpentine electrodes can be extended up to 70%, the maximal applied strain in this study was limited to 30% as it corresponds to the typical standard value used for the most of current applications. In order to demonstrate the advanced stretchable features of the 3D geometry, the morphology of LTO micropillars under stretched condition has been examined and compared to that of a continuous LTO layer that was 100 μm thick (Fig. 4a and b). The SEM images taken under a 30% tensile strain bring out the superior mechanical behavior of micropillars. Indeed, continuous LTO film on serpentines reveal the presence of several cracks and delamination of the film occurs while vertical micropillar structures can support the mechanical deformations thanks to empty spaces surrounding them. In addition, adhesion of micropillars on Al is absolutely not affected by the mechanical constraint. It can be noted that

Table 1
Electrochemical performance comparison between 3D and 2D Li-ion stretchable microbatteries.

Configuration	3D microbattery		2D microbattery	
C-rate	C/10	C/2	C/10	C/2
Discharge capacity (mA h cm^{-2})				
1st cycle	2.51	0.95	1.02	0.41
2nd cycle	2.40	0.87	0.94	0.36
50th cycle	2.26	0.80	0.92	0.31
Capacity retention at 50th cycle (%)	94	92	97	86
Areal energy (mW h cm^{-2})				
1st cycle	6.27	2.37	2.55	1.02
2nd cycle	6.00	2.17	2.35	0.90
50th cycle	5.65	2.00	2.30	0.77
Areal Power (mW cm^{-2})				
1st cycle	0.62	1.18	0.25	0.51
2nd cycle	0.60	1.08	0.35	0.90
50th cycle	0.56	1.00	0.23	0.77
3D gain factor (G_{3D})				
1st cycle	2.46	2.31	–	–
2nd cycle	2.55	2.42	–	–
50th cycle	2.45	2.58	–	–

the serpentines are slightly detached from the PDMS substrate because the electrodes have not been encapsulated for making SEM examinations possible. In Fig. 4c, it is given the electrochemical performance of the 3D and the 2D microbatteries carried out at 1C under different tensile stress varying from 0% to 30%. Although the 2D microbattery can be stretched, the discharge capacity suffers from an abrupt drop of 33% followed by a continuous fade during the next following 30 cycles as a 10% tensile strain is applied after the 30th discharge cycle. The capacity retention was estimated to reach only 26% after 60 electrochemical cycles under such a short elongation. This tendency is even more accentuated when the battery is stretched up to 20% attaining a negligible capacity retention of 2% at the 90th cycle. At a stretching of 30%, the discharge capacity is zero suggesting that the battery does not work anymore. In addition, the created damages are irreversible as it is confirmed by the negligible capacity values obtained from the following electrochemical tests that have been performed under relaxed condition. Such a low stretchability of the 2D configuration is attributed to the weak mechanical properties of the active material used in the layer form leading to its delamination and the total loss of the electrical contact with the current collector. For the 3D microbattery, the influence of different strains has only a limited effect on the electrochemical properties. Indeed, 83% of the capacity is retained at the 60th discharge under 10% strain. The small capacity fading can be attributed to the detachment of few micropillars from the serpentine current collectors (see the SEM image of 3D LTO electrodes that was taken under 30% strain in Fig. S3). Delamination of individual micropillars has been also evidenced by the slight increase of the internal resistance when the battery is stretched up to 30% (see the EIS spectra in Fig. S4).

Compared to the 2D configuration, discharge capacity values slowly decrease under stronger mechanical stress. Actually, the capacity retention is varying from 76% at the 90th cycle under 20% strain to 73% at the 120th discharge cycle under 30% strain. Even remarkable, the capacity slightly increased after releasing the 3D microbattery to its original state and its capacity retention attained 77% at the 150th cycle under relaxed conditions. Finally, compared to the electrochemical performance of the microbattery along 150 charge/discharge cycles at zero strain (Fig. 3e), the 3D microbattery showed nearly similar electrochemical performance under hard mechanical strains conditions. The good electrochemical and mechanical properties without any alteration of the 3D microbattery are confirmed by the optical images of a red light emitting diode powered under strain of 0% and 30% strain (Fig. 4d). It can be also pointed out that the red diode is lighted-up when the 3D microbattery is also completely folded as seen in Fig. 4e. The above results confirm the advantage of electrodes carrying micropillars which present empty spaces that prevent the formation of cracks under mechanical strain

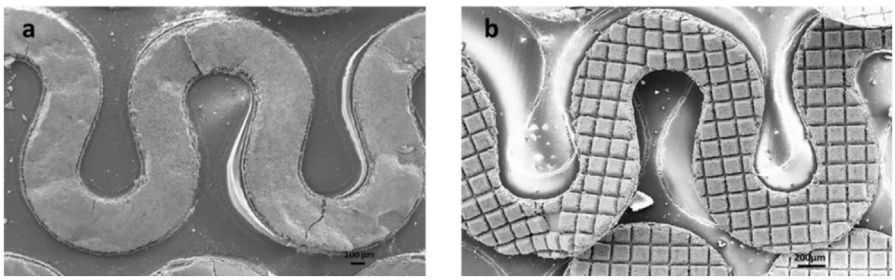

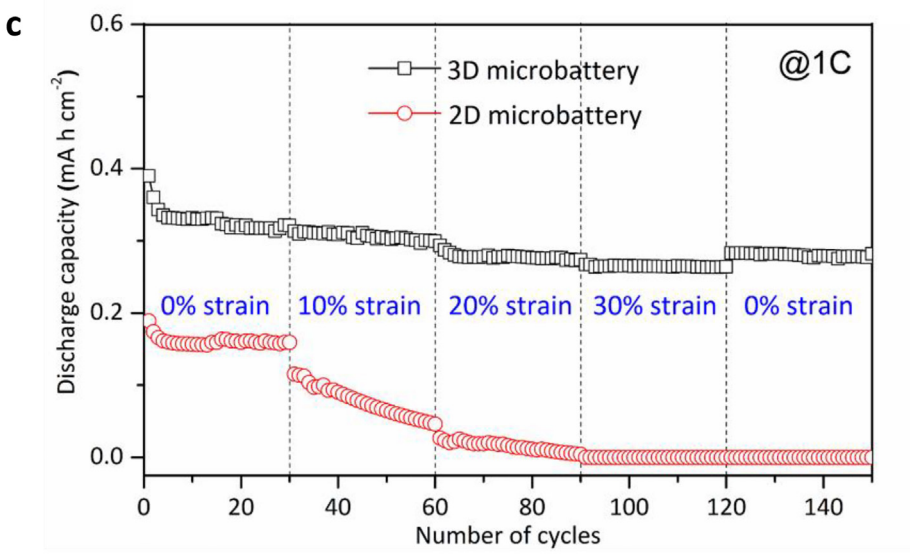

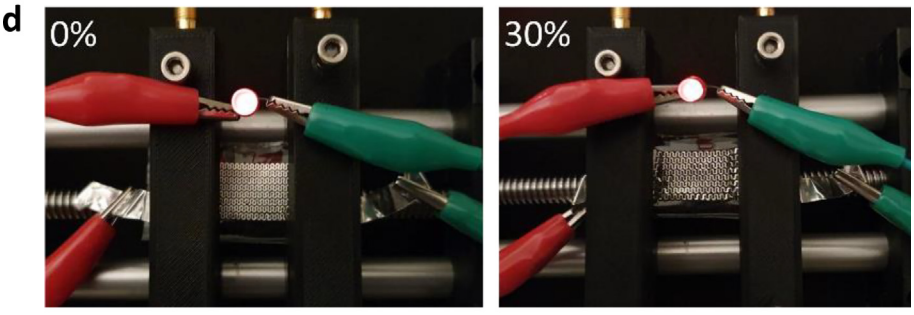

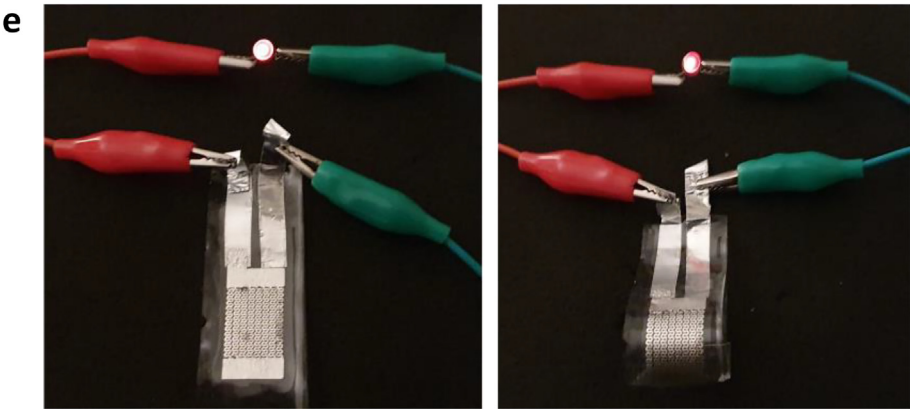

Fig. 4. SEM images of stretched serpentines supporting LTO electrodes a) as a continuous film b) as micropillars. c) Electrochemical performance of the 3D and the 2D microbatteries under different tensile stress varying from 0% to 30% recorded at 1C for 150 charge/discharge cycles. d) 3D microbattery lighting up a red light emitting diode in flat and stretched configurations. e) Optical image of the 3D microbattery powering the red diode under flat and bent configurations. (For interpretation of the references to colour in this figure legend, the reader is referred to the Web version of this article.)

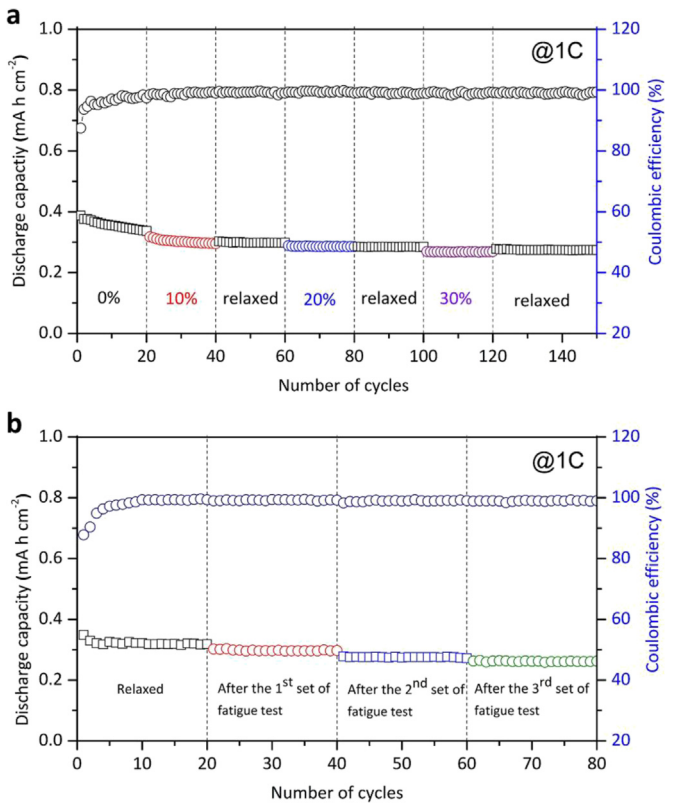

Fig. 5. Mechanical performance of the stretchable 3D microbattery. a) Discharge capacities recorded at 1C for 150 cycles under various tensile strains followed alternatively by relaxed conditions. b) Discharge capacities measured at 1C for 80 cycles after 3 sets of fatigue tests (20 stretch repetitions at 20% strain each).

conditions and the subsequent delamination of the active materials.

To further demonstrate the robustness and reliability of the stretchable microbattery, electrochemical performance tests at 1C have been performed under different conditions. First, discharge capacities delivered by the 3D microbattery that was subjected to strains of 10%, 20%, and 30% followed alternatively by relaxed conditions were recorded for 20 electrochemical cycles each (Fig. 5a). The results show that the discharge capacities are comparable to that obtained in Fig. 4c. A capacity fading corresponding to 27% of the initial capacity is observed. However, the capacity loss is clearly irreversible due to the probable detachment of few micropillars from the current collectors. For more clarity, all detailed values are given in Table 2. The second type of mechanical tests was consisted of measuring the discharge capacities over 20 cycles after 3 sets of fatigue tests that were 20 stretch repetitions at strain of 20% each (Fig. 5b).

Clearly, the impact of this mechanical test on the electrochemical performance is also not really significant as the capacity retention is estimated to attain 90%, 83%, and 80% at end of each set. Moreover, one can notice that CE values remain rather high for all tests (>99.0%). All these results confirm that the 3D microbattery can be handled not only under stretched conditions but also after multiple mechanical strain repetitions with almost no strong influence on the electrochemical characteristics.

Table 2
Mechanical performance of the 3D microbattery (from Fig. 5a).

Strain (%)	10	0	20	0	30	0
Discharge cycle (#)	40	60	80	100	120	150
Capacity (mA h cm^{-2})	0.29	0.29	0.28	0.28	0.27	0.27
Capacity retention (%)	78	79	75	76	71	73
Coulombic efficiency (%)	99.0	99.0	99.2	99.1	99.2	99.4

Table 3
Performance of the main typical stretchable batteries reported in literature.

Design	Type	Energy density mW h cm^{-2}	Max. Strain	Capacity retention at the max strain	References
Self-supported micropillars	Li-ion	6.27	30%–70%	73%	This work
Serpentines from helical springs	Ag–Zn	5.25	100%	100%	[28]
Fiber-shaped/ coplanar	Zn–MnO_2	5.8	100%	100%	[21]
Origami	Li-ion	0.53	1300%	100%	[24]
Arched structure	Li-ion	2.64	450%	97%	[26]
Wavy	Li-ion	7.92	50%	91%	[25]
Rigid islands	Li-ion	2.65	300%	80%	[29]
3D porous sponge	Li-ion	1.87	80%	75%	[22]
Honeycomb	Li-ion	9.18	50%	94%	[27]
Porous sponge	Na-ion	1.56	50%	88%	[23]

The main properties of the stretchable microbattery disclosed in this work are on par with that reported from other typical systems (see the performance comparison in Table 3).

4. Conclusion

In summary, A new stretchable Li-ion microbatteries have been fabricated using an innovative concept. The approach relies on the assembling of two stretchable substrates carrying arrays of micropillar electrodes supported on metallic serpentine and being separated by a gel-polymer electrolyte. We show that unlike compact and continuous thin-films, electrodes composed of vertical micropillar structures supported on serpentines can enhance by 2.5 times the discharge capacity of the microbattery. Also, they can be stretched at different strain configurations showing stable electrochemical performance with a high-rate capability thanks to the empty spaces between pillars that can bear strong mechanical strains. The approach is quite promising as electrochemical and mechanical performances of the 3D microbattery can still be improved by e.g. increasing the density of micropillars and combining other electrode and electrolyte materials.

Credit author statement

Mohamed Nasreldin: Investigation, Formal analysis, **Writing - original draft, Writing - review & editing.**

Roger Delattre: **Supervision, Conceptualization, Writing - review & editing.**

Cyril Calmes: **Help in investigation.**

Marc Ramuz: Help in investigation.

Vinsensia Ade Sugiawati: Help in investigation, Writing - review & editing.

Sébastien Maria: Help in Formal analysis.

Jean-Louis de Bougrenet de la Tocnaye: Writing-Reviewing and Editing.

Thierry Djenizian: Supervision, Conceptualization, Methodology, Writing-Reviewing and Editing.

All of the authors discussed the results and commented on the manuscript. All authors have given approval to the final version of the manuscript.

Declaration of competing interest

The authors declare that they have no known competing financial interests or personal relationships that could have appeared to influence the work reported in this paper.

Acknowledgements

We thank Mines-Saint-Etienne, and the Indo French Centre of the Promotion of Advanced Research for the financial supports.

Appendix A. Supplementary data

Supplementary data to this article can be found online at https://doi.org/10.1016/j.ensm.2020.07.005.

References

[1] C. Lethien, J. Le Bideau, T. Brousse, Energy Environ. Sci. 12 (2019) 96–115.
[2] S. Ouendi, C. Arico, F. Blanchard, J.-L. Codron, X. Wallart, P.L. Taberna, P. Roussel, L. Clavier, P. Simon, C. Lethien, Energy Storage Materials 16 (2019) 581–588.
[3] M. Timmermans, N. Labyedh, F. Mattelaer, S. Zankowski, S. Deheryan, C. Detavernier, P. Vereecken, J. Electrochem. Soc. 164 (2017) D954–D963.
[4] Y. Zhang, Y. Zhao, J. Ren, W. Weng, H. Peng, Adv. Mater. 28 (2016) 4524–4531.
[5] S. Pan, J. Ren, X. Fang, H. Peng, Adv. Energy Mater. 6 (2016) 1501867.
[6] C. Yan, P.S. Lee, Small 10 (2014), 3442–3442.
[7] K. Jost, G. Dion, Y. Gogotsi, J. Mater. Chem. A 2 (2014) 10776.
[8] K. Xie, B. Wei, Adv. Mater. 26 (2014) 3592–3617.
[9] Q. Cheng, Z. Song, T. Ma, B.B. Smith, R. Tang, H. Yu, H. Jiang, C.K. Chan, Nano Lett. 13 (2013) 4969–4974.
[10] L. Hu, H. Wu, F. La Mantia, Y. Yang, Y. Cui, ACS Nano 4 (2010) 5843–5848.
[11] C. Wang, D. Li, C.O. Too, G.G. Wallace, Chem. Mater. 21 (2009) 2604–2606.
[12] B. Yao, J. Zhang, T. Kou, Y. Song, T. Liu, Y. Li, Adv. Sci. 4 (2017) 1700107.
[13] C. Botas, D. Carriazo, G. Singh, T. Rojo, J. Mater. Chem. A 3 (2015) 13402–13410.
[14] Z. Zhou, H. Zhang, Y. Zhou, H. Qiao, A. Gurung, R. Naderi, H. Elbohy, A.L. Smirnova, H. Lu, S. Chen, Q. Qiao, Sci. Rep. 7 (2017).
[15] Z. Chen, W. Ren, L. Gao, B. Liu, S. Pei, H.-M. Cheng, Nat. Mater. 10 (2011) 424–428.
[16] U. Gulzar, S. Goriparti, E. Miele, T. Li, G. Maidecchi, A. Toma, F. De Angelis, C. Capiglia, R.P. Zaccaria, J. Mater. Chem. A 4 (2016) 16771–16800.
[17] U. Gulzar, F. De Angelis, R.P. Zaccaria, C. Capiglia, World J. Textil. Eng. Technol. 2 (2016) 6–15.
[18] S. Zhai, H.E. Karahan, L. Wei, Q. Qian, A.T. Harris, A.I. Minett, S. Ramakrishna, A.K. Ng, Y. Chen, Energy Storage Materials 3 (2016) 123–139.
[19] Q. Huang, D. Wang, Z. Zheng, Adv. Energy Mater. 6 (2016) 1600783.
[20] X. Pu, L. Li, H. Song, C. Du, Z. Zhao, C. Jiang, G. Cao, W. Hu, Z.L. Wang, Adv. Mater. 27 (2015) 2472–2478.
[21] A.M. Gaikwad, A.M. Zamarayeva, J. Rousseau, H. Chu, I. Derin, D.A. Steingart, Adv. Mater. 24 (2012) 5071–5076.
[22] W. Liu, Z. Chen, G. Zhou, Y. Sun, H.R. Lee, C. Liu, H. Yao, Z. Bao, Y. Cui, Adv. Mater. 28 (2016) 35783583.
[23] H. Li, Y. Ding, H. Ha, Y. Shi, L. Peng, X. Zhang, C.J. Ellison, G. Yu, Adv. Mater. 29 (2017) 1700898.
[24] Z. Song, T. Ma, R. Tang, Q. Cheng, X. Wang, D. Krishnaraju, R. Panat, C.K. Chan, H. Yu, H. Jiang, Nat. Commun. 5 (2014).
[25] W. Liu, J. Chen, Z. Chen, K. Liu, G. Zhou, Y. Sun, M.-S. Song, Z. Bao, Y. Cui, Advanced Energy Materials, 2017, p. 1701076.
[26] W. Weng, Q. Sun, Y. Zhang, S. He, Q. Wu, J. Deng, X. Fang, G. Guan, J. Ren, H. Peng, Adv. Mater. 27 (2015) 1363–1369.
[27] S. Kang, S.Y. Hong, N. Kim, J. Oh, M. Park, K.Y. Chung, S.S. Lee, J. Lee, J.G. Son, ACS Nano 14 (2020) 3660–3668.
[28] A.M. Zamarayeva, A.E. Ostfeld, M. Wang, J.K. Duey, I. Deckman, B.P. Lechêne, G. Davies, D.A. Steingart, A.C. Arias, Sci. Adv. 3 (2017), e1602051.
[29] S. Xu, Y. Zhang, J. Cho, J. Lee, X. Huang, L. Jia, J.A. Fan, Y. Su, J. Su, H. Zhang, H. Cheng, B. Lu, C. Yu, C. Chuang, T. Kim, T. Song, K. Shigeta, S. Kang, C. Dagdeviren, I. Petrov, P.V. Braun, Y. Huang, U. Paik, J.A. Rogers, Nat. Commun. 4 (2013) 1543.
[30] D.G. Mackanic, T.-H. Chang, Z. Huang, Y. Cui, Z. Bao, Chemical Society Review, 2020, https://doi.org/10.1039/d0cs00035c. Epub 2020 Jun 02.
[31] S. Park, W.-J. Song, S. Yoo, G. Song, S. Lee, M. Kong, J. Rim, U. Jeong, Batteries Supercaps 2 (2019) 181–199.
[32] Q. Wang, X. Liu, Z. Cui, X. Shangguan, H. Zhang, J. Zhang, K. Tang, L. Li, X. Zhou, G. Cui, Electrochim. Acta 337 (2020) 135843.
[33] A. Mauger, C.M. Julien, A. Paolella, M. Armand, K. Zaghib, Materials 12 (2019) 3892.
[34] B. Commarieu, A. Paolella, J.-C. Daigle, K. Zaghib, Curr. Opin. Electrochem. 9 (2018) 56–63.
[35] A. Mauger, C.M. Julien, A. Paolella, M. Armand, K. Zaghib, Mater. Sci. Eng. R 134 (2018) 1–21.
[36] S. Brutti, G. Greco, P. Reale, S. Panero, Electrochim. Acta 106 (2013) 483–493.
[37] W.K. Pang, N. Sharma, V.K. Peterson, J.-J. Shiu, S. Wu, J. Power Sources 246 (2014) 464–472.
[38] N. Plylahan, M. Letiche, M. Barr, B. Ellis, S. Maria, T.N.T. Phan, E. Bloch, P. Knauth, T. Djenizian, J. Power Sources 273 (2015) 1182–1188.
[39] B. Commarieu, A. Paolella, S. Collin-Martin, C. Gagnon, A. Vijh, A. Guerfi, K. Zaghib, J. Power Sources 436 (2019) 226852.
[40] B. Ellis, P. Knauth, T. Djenizian, Adv. Mater. 26 (2014) 3368–3397.
[41] R. Kohler, H. Besser, M. Hagen, J. Ye, C. Ziebert, S. Ulrich, J. Proell, W. Pfleging, 17(2011) 225–232.
[42] C. Wang, L. Taherabadi, G. Jia, S. Kassegne, J.V. Zoval, M.J. Madou, MEMS, MOEMS, and micromachining, in: Book Series: SPIE 5455, 2004, pp. 295–302.